ELSEVIER

Chemical Engineering Science 61 (2006) 2921–2929

Chemical Engineering Science

www.elsevier.com/locate/ces

CFD simulation of mixing in tall gas–liquid stirred vessel: Role of local flow patterns

A.R. Khopkar[a], G.R. Kasat[b], A.B. Pandit[b], V.V. Ranade[a,*]

[a]*Industrial Flow Modelling Group, National Chemical Laboratory, Pune 411008, India*
[b]*Chemical Engineering Division, University Institute of Chemical Technology, Mumbai 400 019, India*

Received 30 June 2005; received in revised form 22 September 2005; accepted 23 September 2005
Available online 6 January 2006

Abstract

In this work, we have used the computational fluid dynamics (CFD)-based models to investigate the gas–liquid flows generated by three down-pumping pitched blade turbines. A two-fluid model along with the standard k–ε turbulence model was used to simulate the dispersed gas–liquid flow in a stirred vessel. Appropriate drag corrections to account for bulk turbulence [Khopkar and Ranade, 2005. CFD simulation of gas–liquid flow in a stirred vessel: VC, S33 and L33 flow regimes. A.I.Ch.E. Journal, accepted for publication] were developed to correctly simulate different flow regimes. The computational snapshot approach was used to simulate impeller rotation and was implemented in the commercial CFD code, FLUENT4.5 (of Fluent. Inc., USA). The computational model has successfully captured the flow regimes as observed during experiments. The particle trajectory simulations were then carried out to examine the influence of the different flow regimes on the circulation time distribution. The model predictions were verified by comparing the predicted results with the experimental data of [Shewale and Pandit, 2006. Studies in multiple impeller agitated gas–liquid contactors. Chemical Engineering Science 61, 489–504]. The computational model and results discussed in this study would be useful for explaining the implications local flow patterns on the mixing process and extending the applications of CFD models for simulating large multiphase stirred reactors.

Keywords: Stirred vessel; Pitched blade turbine; CFD; Flow regimes; Mixing

1. Introduction

Gas–liquid stirred reactors are widely used in chemical process industry to carry out gas–liquid reactions. In most of the industrial applications, tall reactors equipped with multiple impellers are increasingly used. The multiple impeller system provides better gas utilization, higher interfacial area and narrower residence time distribution in the flow system compared to a single impeller system. Also the multiple impeller systems are preferred in bioreactor, as they offer lower average shear as compared to single impeller system due to overall lower operational speed with nearly same power input and allow more degrees of freedom for controlling the gas dispersion as well as the bulk flow of liquid phase.

In multiple impeller gas–liquid stirred reactor, different gas flow regimes are realized in the reactor depending upon the reactor hardware and operating parameters such as impeller design, impeller spacing, rotational speed and the volumetric gas flow rate. These different flow regimes show different fluid dynamic conditions in the reactor and therefore, can have different rates of transport as well as mixing processes. It is therefore, essential to have better understanding of the influence of reactor hardware as well as operating parameters on the fluid dynamics, to manipulate and to have better control on the performance of the reactor.

Recently, Shewale and Pandit (2006) have experimentally studied the mixing process occurring in an aerated stirred reactor equipped with three down-pumping six-blade pitched turbine operating in different gas flow regimes. They have found significant influence of the prevailing gas flow regimes on the time scale of the mixing process occurring in the reactor. They observed that the change in the flow regime significantly alters

* Corresponding author. Tel.: +91 20 2589 3400; fax: +91 20 2589 3260.
E-mail address: vv.ranade@ncl.res.in (V.V. Ranade).

0009-2509/$ - see front matter © 2005 Elsevier Ltd. All rights reserved.
doi:10.1016/j.ces.2005.09.023

the rates of liquid-phase mixing process. For extending their results to industrial systems, it is essential to develop computational models, which can quantitatively predict the influence of hardware and operating parameters on liquid-phase mixing. In this work, such an attempt is made.

Several attempts have been made in recent years to develop computational models of gas–liquid flows in stirred vessels (for example, Gosman et al., 1992; Bakker and van den Akker, 1994; Ranade and van den Akker, 1994; Ranade and Deshpande, 1999; Lane et al., 2000, 2005; Khopkar et al., 2003, 2005; Khopkar and Ranade, 2005). Most of these studies were restricted to single impeller system. Simulations with multiple impeller system at different flow regimes are rare due to increased complexity and due to unavailability of experimental data. In this work, we made an attempt to develop a CFD model to capture these flow regimes. The computational snapshot approach (Ranade, 2002) was used to simulate impeller rotation. Turbulent dispersed two-phase flow in stirred vessels was simulated using a two-fluid model with the standard k–ε turbulence model. The predicted gross characteristics of the fluid dynamics were compared with the experimental measurements of the Shewale and Pandit (2006). The particle trajectory simulations were then carried out to obtain the Lagrangian information (circulation time distribution) of the liquid phase. The obtained information on circulation time was then used to explain the implications of the liquid flow patterns on the mixing process. The computational model and the predicted results discussed in this work will be useful for providing better understanding of flow characteristics and mixing process occurring in tall aerated stirred reactor operating in different gas flow regimes.

2. Computational model

2.1. Model equations

A two-fluid model was used to simulate the turbulent gas–liquid flows in stirred vessel. The Reynolds averaged mass and momentum balance equations for each phase in turbulent flow regime were written as (without considering mass transfer and turbulent dispersion of bubbles)

$$\frac{\partial(\alpha_q\rho_q)}{\partial t} + \nabla\cdot(\alpha_q\rho_q\overrightarrow{U}_{q,i}) = 0, \tag{1}$$

$$\frac{\partial(\alpha_q\rho_q\overrightarrow{U}_{q,i})}{\partial t} + \nabla\cdot(\alpha_q\rho_q\overrightarrow{U}_{q,i}\times\overrightarrow{U}_{q,i}) = -\alpha_q\nabla\overrightarrow{p} - \nabla\cdot(\alpha_q\overline{\overline{\tau}}^{(lam)}_{q,ij}) - \nabla\cdot(\alpha_q\overline{\overline{\tau}}^{(t)}_{q,ij}) + \alpha_q\rho_q g_i + \overrightarrow{F}_{12,i}. \tag{2}$$

For more details of balance equations, the reader is referred to Ranade (2002).

The standard k–ε turbulence model was used in the present study for simulating turbulent gas–liquid flows in stirred vessels. The governing equations for turbulent kinetic energy, k and turbulent energy dissipation rate, ε, were solved only for the liquid phase and are listed below

$$\frac{\partial}{\partial t}(\alpha_l\rho_l\phi_l) + \nabla\cdot(\alpha_l\rho_l\overrightarrow{U}_{l,i}\phi_l) = -\nabla\cdot\left(\alpha_l\frac{\mu_{tl}}{\sigma_{\phi l}}\nabla\phi_l\right) + S_{\phi,l}, \tag{3}$$

where ϕ_l can be turbulent kinetic energy or turbulent energy dissipation rate in liquid phase. The symbol $\sigma_{\phi l}$ denotes turbulent Prandtl number for variable ϕ. $S_{\phi l}$ is the corresponding source term for ϕ in liquid phase. Source terms for turbulent kinetic energy and dissipation can be written as

$$S_{kl} = \alpha_l\rho_l[(G_l + G_{el}) - \varepsilon_l],$$

$$S_{\varepsilon,l} = \alpha_l\rho_l\frac{\varepsilon_l}{k_l}[C_1(G_l + G_{el}) - C_2\varepsilon_l], \tag{4}$$

where G_l is turbulence generation in liquid phase and G_{el} is extra generation (or dissipation) of turbulence in liquid phase. Generation due to mean velocity gradients, G_l and $\mu_{t,l}$, turbulent viscosity are calculated as

$$G_l = \tfrac{1}{2}\mu_{tl}(\nabla\overrightarrow{U}_{l,i} + (\nabla\overrightarrow{U}_{l,i})^{\mathrm{T}})^2, \quad \mu_{tl} = \frac{\rho_l C_\varpi k_l^2}{\varepsilon_l}. \tag{5}$$

Extra-generation or damping of turbulence due to the presence of dispersed phase particles is represented by G_{el}. In stirred vessel, impeller rotation generates significantly higher turbulence than the turbulence generated due to bubbles; therefore, the contribution of the additional turbulence generation due to bubbles can be neglected. In the present study, therefore, the value of G_{el} was set to zero. Standard values of the k–ε model parameters were used in the present simulations. No separate equations were solved for modeling turbulence in the dispersed phase. Instead the turbulent viscosity of the dispersed phase was estimated from the knowledge of turbulent viscosity of liquid phase as

$$\mu_{tg} = \frac{\rho_g}{\rho_l}\mu_{tl}. \tag{6}$$

The inter-phase momentum exchange term, F_{qi} consists of four forces: the Basset force, the virtual mass force, the lift force and the interphase drag force. Recently, Khopkar and Ranade (2005) studied the influence of different interphase forces on the predicted gas hold-up distribution. Following their recommendations, only the inter-phase drag force was considered in the inter-phase momentum exchange term. The inter-phase drag force exerted on phase 2 in i-direction is given by

$$F_{qi} = F_{D2i} = -\frac{3\alpha_1\alpha_2\rho_1 C_D(\sum(U_{2i} - U_{1i})^2)^{0.5}(U_{2i} - U_{1i})}{4d_b}. \tag{7}$$

In gas–liquid stirred vessels the interphase drag coefficient, C_D, is a complex function of the drag coefficient in a stagnant liquid, the gas hold-up and prevailing turbulence. Recently, Khopkar and Ranade (2005) studied the effect of turbulence on the drag coefficient (slip velocity). Based on a comparison of the predicted gas volume fraction distribution with the experimental data, they have recommended a turbulence correction factor proposed by Brucato et al. (1998) but with a lower value of the

correlation constant. Following this, we have used the following correlation (Eq. (8)) for calculation of the drag coefficient:

$$\frac{C_D - C_{D0}}{C_{D0}} = K\left(\frac{d_b}{\lambda}\right)^3,$$

$$C_{D0} = \max\left\{\left(\frac{2.667Eo}{Eo+4.0}\right), \left(\frac{24}{Re_b}(1+0.15Re_b^{0.687})\right)\right\}, \quad (8)$$

where λ is the Kolmogorov length scale, d_b is the bubble diameter and K is an empirical constant, which was set to 6.5×10^{-06} (Khopkar and Ranade, 2005). Eq. (8) thus accounts for the increased drag coefficient due to turbulence.

The gas–liquid flow in the stirred vessel was simulated using the computational snapshot approach. In this approach, the impeller blades are considered as fixed at one particular position (similar to taking a snapshot of the rotating impeller) with respect to the baffles. Recently, Ranade (2002) discussed the development of the snapshot approach in detail and therefore it is not repeated here. In the present study, the gas–liquid flows in a stirred vessel were simulated for a single specific blade position with respect to the baffles. The computational snapshot approach was implemented in the commercial CFD code FLUENT 4.5 (of Fluent Inc., USA) using user-defined subroutines.

2.2. Solution domain

In the present work, the experimental setup used by Shewale and Pandit (2006) was considered. All the relevant dimensions like the impeller diameter, the reactor shape and diameter and so on were the same as the one used by Shewale and Pandit (2006). The system investigated consists of a stirred cylindrical reactor, with a flat bottom (diameter, $T=0.3$ m, height, $H=0.9$ m) with four baffles (width $= T/10 = 0.03$ m) equally spaced around the reactor periphery. The shaft (diameter $d_s = 0.03$ m) of the impeller was concentric with the reactor axis and extended till the bottom impeller. Three down-pumping pitched blade turbines, of diameter $D_i = 0.1$ m, were used for all simulations. The impeller off-bottom clearance for the bottom most impeller was ($C_1 = 0.15$ m, measured from the mid-plane of impeller). The other two impellers were separated from each other with an axial distance of 0.3 m from each other ($C_2 = C_3 = 0.3$ m). The gas was sparged using ring sparger of diameter, $d_{sp}=0.1$ m and was located at 0.075 m from the bottom of reactor.

Considering the geometrical symmetry, half of the reactor was considered as a solution domain (see Fig. 1). The baffles were considered at angles of 45° and 135°. The impeller was positioned in such a way that three blades were located at angles of 30°, 90° and 150° (measured from center line of impeller blade). The computational snapshot approach divides the solution domain into an inner region, in which time derivative terms are approximated using spatial derivatives and an outer region, in which time derivative terms are neglected. The boundary between the inner and outer regions needs to be selected in such a way that the predicted results are not sensitive to its actual location. In the present work, for all the simulations, the boundary of the inner region was positioned at $r = 0.088$ m and $0.095\text{ m} \leqslant z \leqslant 0.82$ m (where z is the axial distance from the bottom of the reactor).

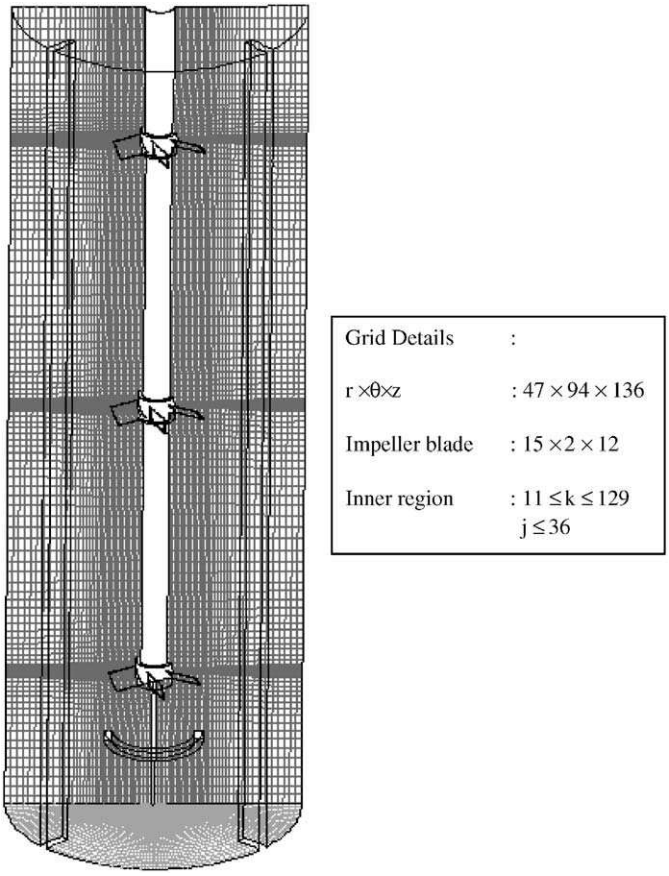

Fig. 1. Computational grid and solution domain.

In the present work, the sparger was modeled as a solid wall. The mass and momentum source of the gas phase was specified one cell above the sparger to simulate gas introduction into the reactor. It must be noted that the volumetric flow rate used in the present study corresponds to the sparger hole velocity of 28 m/s. For such a high hole velocity may lead to jetting. The jets emanating from the sparger will interact with rotating impeller blades. It is however extremely difficult to simulate jetting within the Eulerian–Eulerian (EE) framework used in the present study. None of the published CFD simulations of gas–liquid flows in stirred vessels so far have considered jetting from the sparger. Ideally a separate sub-model to mimic the influence of jets can be incorporated in the EE modeling framework. In the experiments considered in this work, sparger diameter is same as that of impeller. For such a case with down-pumping impeller, the gas jets may be broken up in the vicinity of the sparger. Therefore, we had not incorporated any sub-model for jetting. One of the possible implications of ignoring jetting might be under-prediction of the critical impeller speed required for the dispersion of gas in the vessel.

Special boundary conditions are needed to simulate gas–liquid interface at the top through which bubbles escape the solution domain. Recently, Ranade (2002) has discussed different possible approaches to treat gas–liquid interface in

detail. We have modeled the top surface of the dispersion as a velocity inlet. The outgoing (axial) velocity of gas bubbles was set equal to the terminal rise velocity of gas bubbles (estimated as 0.2 m/s for air bubbles). All the other velocity components for gas and liquid phase were set to zero. The volume fraction specified at the outlet boundary has no influence on the simulated flow results. The mass and momentum conservation equations for the gas phase were solved and the gas distribution within the vessel was predicted. Implicit assumption here is that gas bubbles escape the dispersion with terminal rise velocity. Since the liquid velocity near the top gas–liquid interface is small and the overall volume fraction of gas is also small ($<5\%$), this assumption is reasonable. The boundary condition used at the top surface of the vessel in this work represents a convenient way to represent this within the framework of commercial CFD code FLUENT. Alternative ways give almost the same results with additional computational costs (see Ranade, 2002).

In a gas–liquid stirred reactor, there is a wide distribution of bubble sizes. The prevailing bubble size distribution in a gas–liquid stirred reactor is controlled by several parameters like reactor configuration, impeller speed and gas flow rate. It is possible to develop a detailed multi-fluid computational model using population balance framework to account for bubble size distribution. However, the use of multi-fluid models based on the population balance increase the computational demands by manifolds. Unfortunately, available experimental data of bubble size distribution in stirred reactor is not adequate to calculate the parameters appearing in the coalescence and break-up kernels. Shewale and Pandit (2006) did not measure the bubble size distribution in their experimental stirred vessel. There is very limited experimental data on bubble size distribution is available in literature. Barigou and Greaves (1992) for single impeller system and Alves et al. (2002) for dual impeller system have reported the experimentally measured bubble size distribution in stirred vessel. Their experimental data clearly indicates that the bubble size in the bulk region of the vessel varies between 3 and 5 mm. We have therefore, used effective bubble size as 4 mm for all the three simulations. The corresponding value of Eo number for 4 mm bubble was found to be 2.178. Fluid properties were set to those of water and air for the primary and secondary phases, respectively.

A commercial grid-generation tool, GAMBIT 2.0 (of Fluent Inc., USA) was used to model the geometry and to generate the body-fitted grids. It is very important to use an adequate number of computational cells while numerically solving the governing equations over the solution domain. The prediction of turbulence quantities is especially sensitive to the number of grid nodes and grid distribution within the solution domain. Following the recommendations of our previous work (Ranade et al., 2001), the numerical simulations for the gas–liquid flows in stirred reactors were carried out for grid size of ($r \times \theta \times z$: $47 \times 94 \times 136$). In the present work, we have used ($r \times \theta \times z$: $15 \times 2 \times 12$) grid nodes to resolve the blade surface. The boundary of the inner region was positioned at $j \leqslant 36$ and $11 \leqslant k \leqslant 129$ (where j is the cell number in the radial direction from the shaft and k is the cell number in the axial direction from the bottom of the reactor). The computational grid used in the present work is shown in Fig. 1.

Differencing of the advection terms has been carried out using the QUICK discretization scheme with the SUPERBEE limiter function (to avoid non-physical oscillations). Standard wall functions were used to specify wall boundary conditions. Different criteria like the reduction of the residuals, gas mass flow rate through various horizontal planes and variation of overall gas hold-up and energy dissipation rates were used to ensure adequate convergence. The validation of computational results with the reported experimental data is discussed in the following section.

3. Results and discussion

3.1. Bulk flow characteristics

The gas–liquid flows generated by three down-pumping pitched blade turbines in a stirred reactor were simulated for a single volumetric gas flow rate (Q_g) of 1.06×10^{-3} m^3/s and for three impeller rotational speeds (N) equal to 100, 145 and 390 rpm, respectively, corresponding to $Fl = 0.638$ & $Fr = 0.028$; $Fl = 0.438$ & $Fr = 0.0597$ and $Fl = 0.163$ & $Fr = 0.430$, respectively. Under these operating conditions, the fluid dynamics in the reactor represents, DFF, DDF and DDL flow regimes, respectively (Shewale and Pandit, 2006), where D represents for fully dispersed condition, L represents for loading condition and F represents for flooding condition. The DFF flow regime corresponds to upper impeller is in dispersed condition and middle and bottom impellers are in flooded condition. The other two flow regimes can also be explained using the same terminology.

The predicted liquid-phase velocity vectors for all the three operating conditions are shown in Fig. 2. It can be seen from Fig. 2 that the computational model captured the significantly different flow fields for all the three conditions. For DFF ($Fl = 0.638$ & $Fr = 0.028$) flow regime, the predicted velocity field shows the presence of two-loop structure. It can be seen that the bottom loop present in the reactor was formed due to the upward rising sparged gas. This upward moving liquid circulation pattern was present till the middle impeller. However, the upper impeller generates a well-known downward moving single circulation loop. Both these circulation loops interact with each other at middle impeller plane.

The predicted liquid-phase velocity field for DDF flow regime ($Fl = 0.438$ & $Fr = 0.0597$) is shown in Fig. 2b. It can be seen from Fig. 2b that the computational model has predicted the two-loop structure for DDF flow regime. However, the predicted two-loop structure for DDF flow regime was significantly different than the two-loop structure predicted for DFF flow regime. The predicted flow pattern shows the presence of a small circulation loop at the bottom of the reactor. This circulation loop was found to be generated due to the dominance of upward rising gas in the region below the bottom impeller and was present till the bottom impeller plane. Whereas, the flow generated by middle and upper impellers were found to interact with each other and form a single

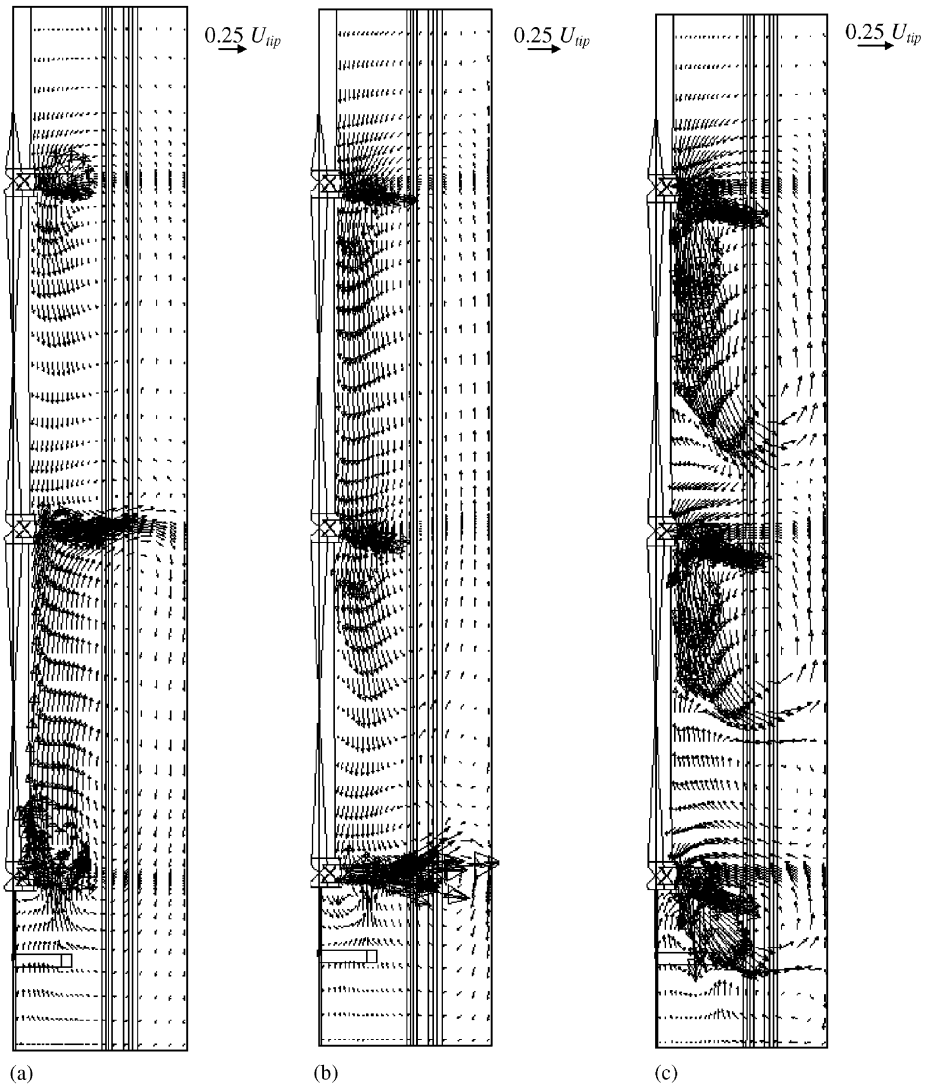

Fig. 2. Predicted mean liquid velocity field at mid-baffle plane for DFF, DDF and DDL flow regimes (a) DFF flow regime($Fl = 0.638 \& Fr = 0.028$), (b) DDF flow regime ($Fl = 0.438 \& Fr = 0.0597$), (c) DDL flow regime($Fl = 0.163 \& Fr = 0.430$).

circulation loop. Along with these two primary circulation loops, the computational model has also captured a secondary circulation loop, present between the both circulation loops. Similarly, the predicted liquid-phase velocity field for DDL flow regime ($Fl = 0.163$ & $Fr = 0.430$) is shown in Fig. 2c. It can be seen that the computational model has predicted three separate circulation loops for each impeller. The predicted velocity field for DDL condition also captured two secondary circulation loops, one at the bottom of the reactor and another between the lower and middle impeller circulation loops. The complex interaction between the impeller-generated flow and gas-generated flow was responsible for the formation of these two secondary circulation loops in the reactor.

The gas hold-up distribution in the reactor is strongly affected by the prevailing flow regime and reactor internals. In the present study, we have used the computational model to study the gas hold-up distribution in DFF, DDF and DDL flow regimes. The qualitative comparison of predicted gas hold-up distributions for all the three operating conditions [$Fl = 0.638$ & $Fr = 0.028$ (DFF); $Fl = 0.438$ & $Fr = 0.0597$ (DDF) and $Fl = 0.163$ & $Fr = 0.430$ (DDL)] with experimental snapshots is shown in Fig. 3. It can be seen from Fig. 3a that similar to experimental condition, the simulation has captured the inefficient dispersion of gas at bottom and middle impeller and dispersed condition of gas at upper impeller for DFF flow regime. The predicted contour plot clearly shows the upward and inward movement of the sparged gas while rising through the reactor till middle impeller. The contour plot shows that there is no effect of rotation of bottom impeller on the upward rising gas. This upward rising gas generates a single circulation loop in the bottom part of the reactor and which was found to be present till middle impeller. The upward rising gas then gets dispersed in the circulation loop generated by an upper impeller.

The qualitative comparison of experimental snapshot of gas–liquid flow and predicted contour plot for the simulated gas hold-up distribution for DDF flow regime is shown in

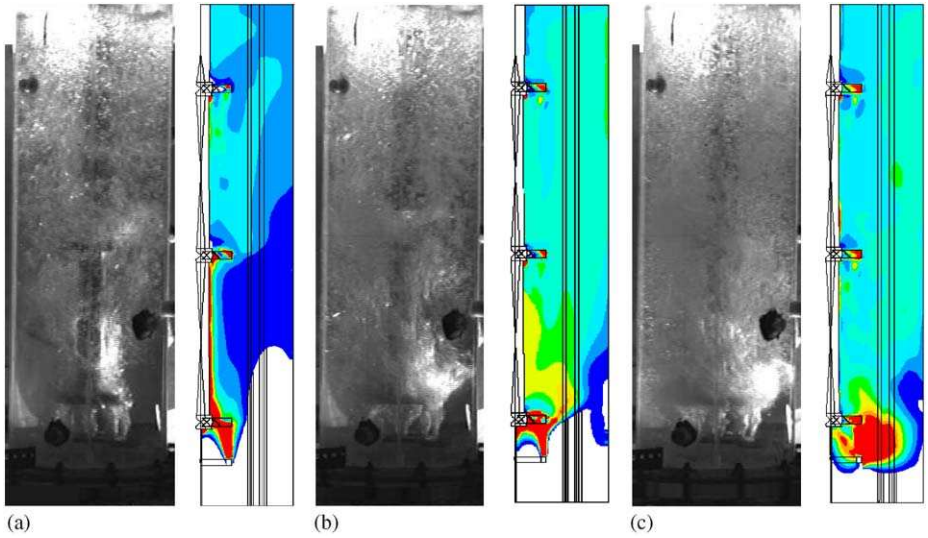

Fig. 3. Qualitative comparison of experimental snapshot and predicted gas hold-up distribution at mid-baffle plane for DFF, DDF and DDL flow regimes (a) DFF flow regime($Fl = 0.638\&Fr = 0.028$), (b) DDF flow regime ($Fl = 0.438\&Fr = 0.0597$), (c) DDL flow regime($Fl = 0.163\&Fr = 0.430$).(10 uniform contours; minium gas volune fraction, blue = 0.015 and maximum gas volume fraction, red$\leqslant$0.15).

Fig. 3b. It can be seen from Fig. 3b that the simulation has captured the inefficient dispersion of gas by the bottom impeller and the complete dispersed conditions by the middle as well as upper impeller as observed in experiments. The impeller motion of the bottom impeller for DDF flow regime was found to be not sufficient to disperse the gas in the lower impeller region. Similarly, the simulated gas hold-up distribution for DDL flow regime and experimental snapshot of gas–liquid flow is shown in Fig. 3c. It can be seen that for DDL flow regime, the predicted gas hold-up distribution shows the fully dispersed condition for upper and middle impeller and loading condition for the bottom impeller.

Predicted influence of gas flow rate on gross characteristics like power number and total gas hold up are also of interest. Power number was calculated from simulated results as

$$N_p = \frac{2\int_V \alpha_l \rho_l \varepsilon \, \mathrm{d}V}{\rho_l N^3 D_i^5}, \tag{9}$$

where D_i is the impeller diameter and N is the impeller speed. The predicted as well as experimentally measured values of power number and total gas hold-up values are listed in Table 1. It can be seen that the computational model over-predicted the values of impeller power number and total gas hold-up. The turbulence model, use of a single bubble size and inadequacies of inter-phase momentum exchange term are some of the possible reasons for the observed over-prediction. One of the key reasons of the observed over-prediction of total gas hold-up might be inaccurate estimation of inter-phase drag force. Knowledge about influence of bubble size, neighboring bubbles and prevailing turbulence on inter-phase drag force is not adequate. Similarly, the prevailing levels of turbulence were estimated using the standard k–ε model of turbulence. In absence of better understanding, single-phase parameters were used and influence of bubbles on turbulence generation was ignored. The use of single-phase parameters might have contributed in the over-prediction of the impeller power number.

Overall, it can be said that the computational model has qualitatively simulated the three different flow regimes prevailing in a tall stirred reactor equipped with three down-pumping pitched blade turbines. The computational model has also captured the influence of the operating conditions/flow regimes on the flow patterns developed in the reactor. Such significant change in the liquid flow pattern may result into different rates of transport and mixing process. Shewale and Pandit (2006) have observed different trends in the mixing time variation with change in the flow regime. The particle trajectory simulations, using Lagrangian approach were carried out to understand the influence of these flow patterns on the circulation time distribution.

3.2. Mixing in gas–liquid stirred reactor

Mixing time and circulation time are the two criteria used to characterize the liquid-phase mixing in stirred reactors. Mixing time is the time required to achieve a certain degree of homogeneity (Ranade et al., 1991). Whereas circulation time is the time necessary for a fluid element to complete a one circulation within the vessel (time difference between an event of fluid element exiting from the impeller swept volume and an event of its re-entry into impeller swept volume). The link between these two parameters is clear: lower the circulation time for particles to circulate in the reactor, the more efficient is the mixing. In common practice, mixing time is usually taken as some multiple of average circulation time (Joshi et al., 1982). In the present study, we have used the circulation time criteria to investigate the prevailing mixing process.

Table 1
Gross characteristics of a tall gas–liquid stirred reactor (experimental data from Shewale and Pandit, 2006)

Flow regime	Total gas hold-up (%)		Power number, N_{Pg}		Average circulation time, t_c (predicted)	Mixing time, t_m (experimental)	Percentage change	
	Predicted	Experimental	Predicted	Experimental			$t_c/t_{c\,\min}$	$t_m/t_{m\,\min}$
DFF ($Fl = 0.6328$ & $Fr = 0.028$)	2.99	2.47	2.64	2.2	13.851	59	1.493	1.553
DDF ($Fl = 0.438$ & $Fr = 0.0597$)	3.43	2.79	2.98	2.55	9.277	38	1	1
DDL ($Fl = 0.163$ & $Fr = 0.430$)	5.58	3.65	4.05	3.45	11.234	45	1.211	1.184

Using the Eulerian flow field obtained as discussed in previous subsection, the particle trajectories were simulated. The particle trajectory simulations were carried out for three operating conditions [$Fl = 0.638$ & $Fr = 0.028$ (DFF)], [$Fl = 0.438$ & $Fr = 0.0597$ (DDF)] and [$Fl = 0.163$ & $Fr = 0.43$ (DDL)]. A single neutrally buoyant particle (density equals with water) was released in liquid for particle trajectory calculation. The size of neutrally buoyant particle may influence the predicted circulation time distribution. Rammohan et al. (2003) numerically studied the influence of particle size on the predicted values of the turbulent kinetic energy. They found that a neutrally buoyant particle of having size 0.25 mm adequately respond to the liquid-phase turbulence. They observed that the ratio of estimated turbulent kinetic energy and to actual kinetic energy was found to be one for particle of having size $\leqslant 0.25$ mm. Therefore in present study, a single neutrally buoyant particle (density equals with water) of diameter 0.25 mm was released in liquid for particle trajectory calculation. The particle was released in liquid at 10 different positions in the solution domain. These 10 particle release locations were selected randomly. The motion of particle in liquid phase was simulated using the Lagrangian framework. The simulated particle trajectories were used to calculate the circulation time distribution. The details of the trajectory calculations are recently discussed by Rammohan et al. (2003) and hence not repeated here.

Before discussing the predicted results, it is essential to first identify the minimum number of circulations required to adequately represent the circulation time distribution in a gas–liquid stirred reactor. The particle trajectory simulations for DDF flow regime were therefore carried out to check the influence of the number circulations on the average circulation time. The preliminary simulations show that the minimum of 100 circulations was essential to reasonably predict the average circulation time (not shown here for brevity). Above 100 circulations, the average circulation time varies only about ±2% about the average circulation time calculated from 500 circulations. In the present study 500 circulations of neutrally buoyant particles were thought to be adequate to explain the circulation time distribution in all the three flow regimes.

The simulated circulation time distributions for all the three operating conditions are shown in Fig. 4. The simulated circulation time distribution was calculated based on 500 circulations of particle. It can be seen from Fig. 4 that for DFF flow regime the simulated circulation time distribution show the presence of 82% of the total circulations with having circulation time lies between 4 and 16 s. It looks that these 82% of circulations were from the particle following the lower circulation loop. The simulated distribution shows the presence of remaining 18% circulations having circulation time higher than 16 s. These circulations were because of the particle following the upper circulation loop and may lead to slower mixing in the reactor. Incidentally for the DFF flow regime almost no circulations (less than 1%) with having circulation time less than 4 s were found in the simulated circulation time distribution.

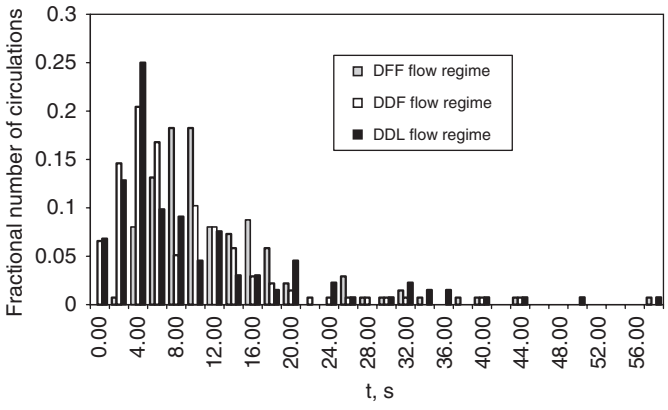

Fig. 4. Predicted circulation time distribution for DFF, DDF and DDL flow regimes.

The simulated circulation time distribution for DDF flow regime is shown in Fig. 4. It can be seen from Fig. 4 that for DDF flow regime, almost 88% of the circulations with having circulation time less than 14 s were present in the simulated distribution. Out of these 88% circulations, almost 60% (in all 500 circulations) were found to have the circulation time less than 6 s. It looks like that these circulations were for the lower circulation loop, which ensures the faster mixing in the lower circulation loop region. The simulated circulation time distribution for DDF flow regime also show the presence of only 5% circulations with having circulation time more than 22 s. Therefore, it can be said that the fluid dynamics in DDF flow regime ensures a faster mixing in the reactor compared to

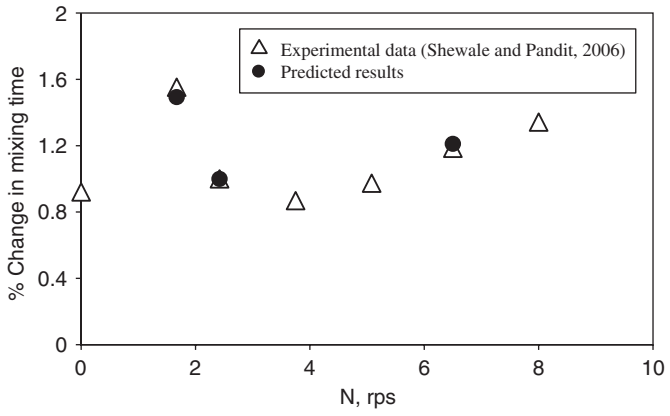

Fig. 5. Comparison of the predicted percentage change in mixing time with experimental data.

the DFF flow regime. Similarly, the simulated circulation time distribution for DDL flow regime is shown in Fig. 4. It can be seen from Fig. 4 that similar to DDF flow regime 63% of the total circulation were found to have circulation time less than 8 s. These circulations were from the particle following the lower circulation loop. However, for DDL flow regime the simulated circulation time distribution shows the presence of 9% circulations with having circulation time more than 30 s. These circulations were because of the particle following the upper circulation loop and may lead to slower mixing in the reactor.

The predicted values of average circulation time and the experimental data are listed in Table 1. Whereas, Fig. 5 shows the variation in the mixing time with changing flow regimes as reported by Shewale and Pandit (2006) and the time required for a fixed number of circulations as per the simulations in this work. It can be seen from Table 1 and Fig. 5 that the predicted values of average circulation time has captured the trends similar to that observed in the experimental study of Shewale and Pandit (2006). The comparison of the increase in predicted average circulation time with respect to predicted minimum average circulation time (for DDF flow regime) was in excellent agreement with the observed rise in the mixing time as reported in the experimental data. Overall, it can be said that the circulation time distribution obtained using quasi-steady-state approach, such as snapshot approach, can indeed explain the implication of the local flow patterns on the mixing process.

The developed computational model not only captured the essential features of the gas–liquid flows operating in different flow regimes but also predicted the implication of the local flow patterns on the overall mixing process with reasonable accuracy. Such validated models will be useful to understand the implication of reactor hardware and scale of operation on the performance. The relative interaction between gas bubbles and impeller blades and mean liquid circulation time change dramatically with changes in the reactor hardware as well as reactor size. The computational model allows one to monitor these changes and allow prediction of their influence on the key transport processes. The model and the results presented here would provide useful basis to allow the extension of computational models to simulate industrial gas–liquid stirred reactors.

3.3. Conclusions

In this work, two-fluid model with the standard k–ε turbulence model was used to simulate the turbulent gas–liquid flows generated by the three down-pumping pitched blade turbines mounted on the same shaft for three operating conditions representing three distinct flow regimes. The computational model qualitatively captured the overall flow field generated by three down-pumping pitched blade turbines, including the liquid circulation loops and the dispersion quality of gas in reactor for all the three flow regimes. It was also found to simulate the variation in the power dissipation by impellers in the presence of the gas and the total gas hold-up reasonably well. The computational model was then used to study the circulation time distribution in the reactor. The predicted circulation time distribution was found to capture the influence of prevailing flow regimes on the mixing process. The predicted percentage change in the circulation time with prevailing flow regimes (DFF, DDF and DDL) showed good agreement with the experimental data.

The computational model shows promising results and seems to be able to predict the gas–liquid flow for any flow regime. The model and results presented in this work would be useful for extending the application of CFD based models for simulating large multiphase stirred reactors.

Notation

C	impeller off-bottom clearance, m
C_D	drag coefficient
d_b	bubble diameter, m
d_{sp}	outer diameter of ring sparger, m
D_i	impeller diameter, m
Eo	Eotvos number, $Eo = g(\rho_l - \rho_g)d_b^2/\sigma_l$
F_D	interphase drag force, N/m^3
Fl	flow number
Fr	Froude number
g	acceleration due to gravity, m/s^2
H	vessel height, m
k	turbulent kinetic energy, m^2/s^2
N	impeller rotational speed, rps
N_P	power number
P	pressure, N/m^2
r	radial coordinate, m
Re_b	bubble Reynolds number
t	time, s
t_c	circulation time, s
t_m	mixing time, s
T	vessel diameter, m
U	velocity, m/s
U_{slip}	slip velocity, m/s
V	volume of vessel, m^3
x	position vector, m
z	axial coordinate, m

Greek letters

α	gas volume fraction
ε	turbulent kinetic energy dissipation rate, m^2/s^3
θ	tangential coordinate
λ	Kolmogorov length scale, m
μ	viscosity, kg/m s
ρ	density, kg/m^3
τ	shear stress, N/m^2

Subscripts

1	liquid
2	gas
q	phasenumber
t	turbulent

Acknowledgements

One of the authors (ARK) is grateful to CSIR for providing research fellowship. The Department of Science and Technology Grant (No. DST/SF/40/99) supported part of the work.

References

Alves, S.S., Maia, C.I., Vasconcelos, J.M.T., 2002. Experimental and modelling study of gas dispersion in a double turbine stirred tank. Chemical Engineering Science 57, 487–496.

Bakker, A., van den Akker, H.E.A., 1994. A computational model for the gas–liquid flow in stirred reactors. Transactions of the Institution of Chemical Engineers 72, 594–606.

Barigou, M., Greaves, M., 1992. Bubble size distribution in a mechanically agitated gas–liquid contactor. Chemical Engineering Science 47 (8), 2009–2025.

Brucato, A., Grisafi, F., Montante, G., 1998. Particle drag coefficient in turbulent fluids. Chemical Engineering Science 45, 3295–3314.

Gosman, A.D., Lekakou, C., Politis, S., Issa, R.I., Looney, M.K., 1992. Multidimensional modelling of turbulent two-phase flows in stirred vessels. A.I.Ch.E. Journal 38 (12), 1947–1956.

Joshi, J.B., Pandit, A.B., Sharma, M.M., 1982. Mechanically agitated gas–liquid reactors. Chemical Engineering Science 37, 813–844.

Khopkar, A.R., Ranade, V.V., 2005. CFD simulation of gas–liquid flow in a stirred vessel: VC, S33 and L33 flow regimes. A.I.Ch.E. Journal, accepted for publication.

Khopkar, A.R., Aubin, J., Xureb, C., Le Sauze, N., Bertrand, J., Ranade, V.V., 2003. Gas–liquid flow generated by a pitched blade turbine: particle velocimetry measurements and CFD simulations. Industrial & Engineering Chemistry Research 42, 5318–5332.

Khopkar, A.R., Rammohan, A., Ranade, V.V., Dudukovic, M.P., 2005. Gas–liquid flow generated by a Rushton turbine in stirred vessel: CARPT/CT measurements and CFD simulations. Chemical Engineering Science 60, 2215–2229.

Lane, G.L., Schwarz, M.P., Evans, G.M., 2000. Modelling of the interaction between gas and liquid in stirred vessels. In: Proceedings of 10th European Conference on Mixing, Delft, The Netherlands, pp. 197–204.

Lane, G.L., Schwarz, M.P., Evans, G.M., 2005. Computational modelling of gas–liquid flow in mechanically stirred tanks. Chemical Engineering Science 60, 2203–2214.

Rammohan, A.R., Duducovic, M.P., Ranade, V.V., 2003. Eulerian flow field estimation from particle trajectories: numerical experiments for stirred type flows. Industrial & Engineering Chemistry Research 42, 2589–2601.

Ranade, V.V., 2002. Computational Flow Modelling for Chemical Reactor Engineering. Academic Press, New York.

Ranade, V.V., van den Akker, H.E.A., 1994. Modelling of flow in gas–liquid stirred vessels. Chemical Engineering Science 49, 5175–5192.

Ranade, V.V., Deshpande, V.R., 1999. Gas liquid flow in stirred reactors: trailing vortices and gas accumulation behind impeller blades. Chemical Engineering Science 54, 2305–2315.

Ranade, V.V., Bourne, J.R., Joshi, J.B., 1991. Fluid mechanics and blending in agitated tanks. Chemical Engineering Science 46, 1883.

Ranade, V.V., Perrard, M., LeSauze, N., Xureb, C., Bertrand, J., 2001. Trailing vortices of Rushton turbines. Chemical Engineering Research and Design 79A, 3.

Shewale, S.D., Pandit, A.B., 2006. Studies in multiple impeller agitated gas–liquid contactors. Chemical Engineering Science 61, 489–504.